**Acknowledgments**

This work was supported by the National Science Foundation under grant number CBT-8502407.

Manuscript submitted May 27, 1988; revised manuscript received Dec. 7, 1990.

*The University of California, Berkeley, assisted in meeting the publication costs of this article.*

REFERENCES

1. J. E. Bauerle, *J. Phys. Chem. Solids*, **30**, 2657 (1969).
2. M. J. Verkerk and A. J. Burggraaf, *This Journal*, **130**, 76 (1983).
3. D. Y. Wang and A. S. Nowick, *ibid.*, **126**, 1166 (1979).
4. A.J. A. Winnubst, A. H. A. Scharenborg, and A. J. Burggraaf, *Solid State Ionics*, **14**, 319 (1984).
5. D. Braunshtein, D. S. Tannhauser, and I. Riess, *This Journal*, **128**, 82 (1981).
6. T. M. Gur, I. D. Raistrick, and R. A. Huggins, *Solid State Ionics*, **1**, 251 (1980).
7. J. Mizusaki, K. Amano, S. Yamauchi, and K. Fueki, in "Chemical Sensors," T. Seiyama, Editor, Elsevier Pub. Co., Amsterdam (1983).
8. E. Schouler and M. Kleitz, *J. Electroanal. Chem.*, **64**, 135 (1975).
9. N. L. Robertson and J. N. Michaels, AIChE Symposium Series 254, Vol. 83, p. 56 (1987).
10. N. L. Robertson and J. N. Michaels, *This Journal*, **137**, 129 (1990).
11. D. Y. Wang and A. S. Nowick, *ibid.*, **126**, 1155 (1979).
12. D. W. Strickler and W. G. Carlson, *J. Am. Ceram. Soc.*, **48**, 286 (1965).
13. S. H. Chu and M. A. Seitz, *J. Solid State Chem.*, **23**, 297 (1978).
14. A. J. Bard and L. R. Faulkner, "Electrochemical Methods," John Wiley & Sons, Inc., New York (1980).
15. A. S. Nowick and D. S. Park, in "Superionic Conductors," G. D. Mahan and W. L. Roth, Editors, Plenum (1976).
16. S. P. S. Badwal, *J. Mater. Sci.*, **19**, 1767 (1984).

# A Mathematical Model for Etching of Silicon Using $CF_4$ in a Radial Flow Plasma Reactor

**Sang-Kyu Park***,[1] **and Demetre J. Economou***

*Department of Chemical Engineering, University of Houston, Houston, Texas 77204-4792*

ABSTRACT

A mathematical model for plasma etching of silicon using tetrafluoromethane in a radial flow reactor was developed. Finite element methods were employed to calculate the two-dimensional flow, temperature, and species concentration fields. Etching rate and uniformity were studied as a function of reactor operating conditions, including the effect of flow direction. For the parameter values examined, the etching rate increased monotonically with flow rate. For low substrate temperature (298 K), inward flow resulted in higher etching rate as compared to outward flow, but the trend reversed at higher temperature. For flow rates greater than 200 sccm, outward flow with a uniform electron density distribution gave the best uniformity results. A one-dimensional radial dispersion approximation was used to study the effect of square-wave power modulation (pulsed-plasma reactor). The etching rate increased with decreasing pulse period and with increasing duty cycle. Under conditions which would result in high depletion of the precursor gas in a continuous-wave reactor (*e.g.*, for low flow rates), the pulsed-plasma reactor can offer substantial improvement in uniformity without sacrificing the etching rate.

Plasma etching and deposition of thin solid films is used extensively in microelectronic device fabrication (1, 2). In plasma processing, a feedstock gas is decomposed in a glow discharge to form highly reactive atoms and radicals. The reactive species interact with the substrate to form volatile products, thereby etching the substrate, or adsorb and react on the substrate to deposit a film. One of the main advantages of plasma processes as compared to thermally driven processes (*e.g.*, CVD) is low-temperature operation. Low-temperature processing becomes increasingly important as microelectronic devices continue to shrink. In addition, for the case of plasma etching, the achievable etch anisotropy is crucial for advanced VLSI and ULSI devices.

Parallel-plate plasma reactors are commonly used in the microelectronics industry. One can distinguish between single-wafer reactors, which can process one wafer at a time, and batch reactors, which can process many wafers simultaneously. A common type of batch reactor is the radial flow reactor of the kind invented by Reinberg (3). Despite the inherently high throughput, the radial flow reactor usually yields much poorer uniformity when compared to the single-wafer reactor. Hence, the search for reactor operating conditions and methods of operation to improve uniformity continues.

Transport and reaction in radial flow reactors has been studied for plasma etching (4-8), as well as plasma deposition (3, 9). In these studies, the effect of operating conditions on the etching (or deposition) rate and uniformity was examined. Typical values for the electron density and energy were assumed, and the glow discharge was not treated. Despite the simplifying assumptions, the above and other works provided some insight into the intricate coupling between transport phenomena and reaction kinetics.

Recently we proposed a pulsed-plasma mode of operation in order to improve the reaction uniformity in both etching and deposition reactors (10, 11). In this mode of operation, power to the plasma is modulated at frequencies (*e.g.*, 100 Hz) much lower than the usual radio frequencies used to excite the discharge. During the power-on fraction of the cycle, the usual RF frequency of 13.56 MHz may be used in order to achieve more efficient gas dissociation and to avoid intense ion bombardment and charging of dielectric surfaces. The improvement in reaction uniformity was most noticeable in cases of appreciable depletion of the feedstock gas as the gas flows and decomposes in the plasma (11). In essence, the pulsed-plasma mode of operation allows for replenishment of the precursor gas during the power-off fraction of the cycle. This alleviates the reactant concentration gradients along the active surface with concomitant improvement in the uniformity. Furthermore, since reaction can take place even during the power-off fraction of the cycle, the time-averaged pulsed-plasma reaction rate, prorated by the duty cycle, may be higher than that of the continuous-wave reactor, under otherwise identical conditions (*e.g.*, equal power level when the plasma is on).

In the present study, etching of silicon using a tetrafluoromethane plasma in a radial flow reactor was investigated. Only chemical etching was considered as was done

* Electrochemical Society Active Member.
[1] Present address: Advanced Products Research and Development Laboratory, Motorola, Incorporated, Austin, Texas 78721.

in previous works (4-9). Both a continuous-wave (cw) and a pulsed-plasma reactor were studied. For the cw reactor, a two-dimensional model for gas flow, temperature, and active species concentration distributions was employed. The effect of flow rate, flow direction, power, and electrode temperature on the etching rate and uniformity was examined. For the pulsed-plasma reactor, a one-dimensional time-dependent radial dispersion model was found adequate. The effect of pulse period and duty cycle was studied.

## Model Formulation

A schematic of the reactor studied is shown in Fig 1. The Reinberg-type (3) axisymmetric reactor has two parallel-plate electrodes, and provisions for gas input and exhaust. The plasma is created in the interelectrode space, and the substrates (wafers) to be etched rest on the lower electrode. In practice, only discrete areas of the lower electrode are covered by substrates. In order to preserve the axisymmetric nature of the problem (no azimuthal dependence), it was assumed that the lower electrode is completely covered with etchable material, except for two ring-shaped areas near the center and the periphery of the lower electrode (see Fig. 1). Two gas flow configurations were examined. In the outward flow configuration, fresh gas entered from the reactor center and flowed radially outward. In the inward flow configuration, the gas flow direction was reversed.

The present study focuses on the effect of reactor operating conditions on the etching rate and uniformity. Emphasis was placed on systems for which chemical etching dominates ion-assisted etching. Therefore, the effect of ion bombardment was neglected. The $CF_4$ plasma etching of silicon was chosen as a model system for analysis since the plasma chemistry is known to a reasonable extent, and chemical etching dominates under the relatively high-pressure ($p \geq 0.5$ torr) conditions examined. The following approach was used. The gas velocity and temperature distributions were first obtained by solving the momentum balance, continuity, and energy balance equations. The velocity and temperature fields were then substituted into the mass balance equations to calculate the reactive species concentration distribution in the reactor. The etching rate and uniformity were then found. The full two-dimensional model was employed to describe the time-invariant operation of the continuous-wave reactor. However, a one-dimensional approximation (radial dispersion model) was found adequate for describing the time-dependent operation of the pulsed-plasma reactor.

*Gas velocity and temperature distribution.*—Under the conditions of interest, the continuum approximation is valid, and the gas flow is laminar and axisymmetric. Assuming a Newtonian fluid, the velocity field was obtained by solving the Navier-Stokes equations

$$\rho_o \mathbf{v} \cdot \nabla \mathbf{v} = \nabla \cdot \tau - \rho_o \mathbf{g} \beta (T - T_o) \quad [1]$$

along with the continuity equation

$$\nabla \cdot \mathbf{v} = 0 \quad [2]$$

Here the tensor $\tau$ is given by

$$\tau = -p\mathbf{I} + \mu[\nabla \mathbf{v} + (\nabla \mathbf{v})^T] \quad [3]$$

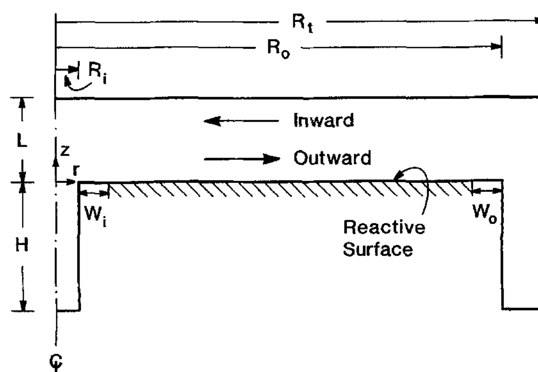


Fig. 1. Schematic of the parallel-plate radial flow reactor studied. Due to symmetry, only half of the reactor is shown. Reactor dimensions are given in Table II.

$\mathbf{I}$ is the identity matrix, $\mathbf{v}$ is the fluid velocity vector, $\rho$ and $\mu$ are the fluid density and viscosity, respectively, $p$ is pressure, $T$ is temperature, $\mathbf{g}$ is the gravitational acceleration vector, subscript o denotes a reference state, and $\beta$ is the thermal expansion coefficient which is given by

$$\beta = \frac{1}{V}\left(\frac{\partial V}{\partial T}\right)_p \quad [4]$$

$V$ being the gas volume. The standard Boussinesq approximation was used, whereby the density was treated as a constant in all terms of the governing equations except for the buoyancy term (last term in Eq. [1]). This approximation seems appropriate for the present system, since the temperature variations in the reactor are relatively small. Density $\rho_o$ was evaluated at a reference temperature $T_o$.

The gas temperature distribution was obtained by solving

$$\rho c_p(\mathbf{v} \cdot \nabla T) = \nabla \cdot (\kappa \nabla T) + G \quad [5]$$

where $c_p$ is the constant-pressure heat capacity, $\kappa$ is the gas thermal conductivity, and G is the energy generated per unit volume of gas. The latter can account for the heat released by volume reactions (*e.g.*, volume recombination) and by gas heating from the plasma. In the present work $G$ was assumed negligible, and was set equal to zero. The momentum, continuity, and energy balance equations are coupled through the temperature dependence of gas viscosity, and through the buoyancy term. The higher the temperature variations in the reactor, the stronger the coupling.

The boundary conditions used for Eq. [1], [2], and [5] are listed below, where the boundary condition number (BC#) refers to the corresponding surface as shown in Fig. 2

BC1 Outflow:

$$v_r = 0, \quad v_z = 2v_{avg}\left[1 - \left(\frac{r}{R_i}\right)^2\right] \quad [6]$$

$$T = T_f \quad [7]$$

BC1 Inflow:

$$v_r = 0, \quad \frac{\partial v_z}{\partial z} = 0, \quad \frac{\partial T}{\partial z} = 0 \quad [8]$$

BC2,4,6,7

$$v_r = 0, \quad v_z = 0, \quad T = T_w \quad [9]$$

BC3

$$v_r = 0, \quad v_z = 0, \quad T = T_s \quad [10]$$

BC5 Outflow:

$$v_r = 0, \quad \frac{\partial v_z}{\partial z} = 0, \quad \frac{\partial T}{\partial z} = 0 \quad [11]$$

BC5 Inflow:

$$v_r = 0, \quad v_z = \frac{2v^*_{avg}}{\left[\frac{1-\lambda^4}{1-\lambda^2} - \frac{1-\lambda^2}{\ln\frac{1}{\lambda}}\right]}\left\{1 - \left(\frac{r}{R_t}\right)^2 + (1-\lambda^2)\frac{\ln\left(\frac{r}{R_t}\right)}{\ln\left(\frac{1}{\lambda}\right)}\right\} \quad [12]$$

$$T = T_f \quad [13]$$

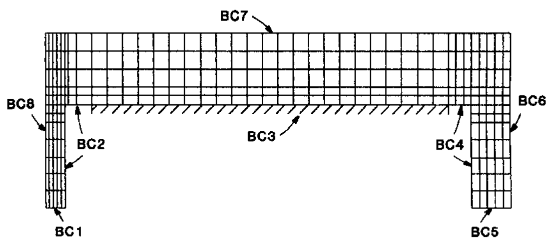


**Fig. 2. The finite element mesh used for calculations. BC# shows the surface over which the corresponding boundary condition was applied.**

**Table I. Rate constants and diffusion coefficients.**

| |
|---|
| $k_{p1} = 6\ 10^{-10}$ cm$^3$/s |
| $k_{p2} = 14\ 10^{-10}$ cm$^3$/s |
| $k_{v1} = 2.53\ 10^{11}$cm$^3$/mol-s |
| $k_{v2} = 7.83\ 10^{12}$ cm$^3$/mol-s |
| $k_{v3} = 4.82\ 10^{12}$ cm$^3$/mol-s |
| $k_{s1} = 4.29\ (T_s)^{0.5}$, $T_s$ in $K$, $k_{s1}$ in cm/s |
| $k_{s2} = 0.438\ (T_s)^{0.5}$, $T_s$ in $K$, $k_{s2}$ in cm/s |
| $k_{s3} = 0.876\ (T_s)^{0.5}$, $T_s$ in $K$, $k_{s3}$ in cm/s |
| $k_n = 97\ (T_s)^{0.5} \exp(-1250/T_s)$, $T_s$ in $K$, $k_n$ in cm/s |
| $D_{F,CF_4} = 3.46\ 10^{-2}\ T^{1.5}/p$, $T$ in $K$, $p$ in torr, $D$ in cm$^2$/s |
| $D_{CF_2,CF_4} = 1.57\ 10^{-2}\ T^{1.5}/p$, $T$ in $K$, $p$ in torr, $D$ in cm$^2$/s |
| $D_{CF_3,CF_4} = 1.07\ 10^{-2}\ T^{1.5}/p$, $T$ in $K$, $p$ in torr, $D$ in cm$^2$/s |
| $D_{CF_4,CF_4} = 9.46\ 10^{-3}\ T^{1.5}/p$, $T$ in $K$, $p$ in torr, $D$ in cm$^2$/s |

BC8 $$v_r = 0, \quad \frac{\partial v_z}{\partial r} = 0, \quad \frac{\partial T}{\partial r} = 0 \qquad [14]$$

Here $\lambda = R_o/R_t$, $v_{avg}$ and $v^*_{avg}$ are the average gas velocities in the reactor inlet duct corresponding to outflow and inflow, respectively (see Eq. [15] and [16] below), $v_z$ and $v_r$ are the axial and radial velocity components, and $z$ and $r$ are the axial and radial coordinates respectively. $T_f$ is the feed gas temperature, $T_s$ is the substrate temperature, and $T_w$ is the reactor wall temperature. Radii $R_i$, $R_o$, and $R_t$ are shown in Fig. 1. The average gas velocities are given by

$$v_{avg} = Q/\pi R_i^2 \qquad [15]$$

$$v^*_{avg} = Q/\pi(R_t^2 - R_o^2) \qquad [16]$$

$$Q = Q_o\ 760\ T_f/(60\ p\ 273) \qquad [17]$$

where $Q$ is the gas flow rate (in cm$^3$/s) at the reactor pressure and inlet temperature conditions. The above boundary conditions include the noslip condition on walls and a constant wall temperature (BC 2, 3, 4, 6, 7), a fully developed laminar flow and a constant gas temperature in the inlet duct (BC1/outflow and BC5/inflow), symmetry conditions along the reactor axis (BC8), and fully developed velocity and temperature profiles at the reactor exit (BC1/inflow and BC5/outflow).

Assuming that the gas is primarily $CF_4$, the gas viscosity, thermal conductivity, and heat capacity were expressed as a function of temperature using published data (12). The above equations provided the gas velocity and temperature distributions in the reactor. Such distributions were then used in the convective diffusion equations to determine the active species concentration profiles as described below.

*Reactive species concentration distribution.*—In silicon etching using a tetrafluoromethane plasma, fluorine atoms are thought to be the main etchant species. In addition, under the relatively high-pressure conditions studied, chemical etching appears to dominate ion-assisted etching. Hence, emphasis was placed on the neutral species chemistry. The chemical reaction model used in the present study was a subset of the reaction set proposed by Ryan and Plumb (13, 14). The following homogeneous (gas phase) reactions were included

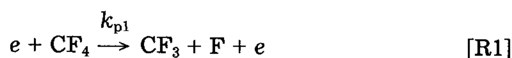

$$e + CF_4 \xrightarrow{k_{p1}} CF_3 + F + e \qquad [R1]$$

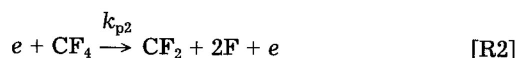

$$e + CF_4 \xrightarrow{k_{p2}} CF_2 + 2F + e \qquad [R2]$$

$$F + CF_2 \xrightarrow{k_{v1}} CF_3 \qquad [R3]$$

$$F + CF_3 \xrightarrow{k_{v2}} CF_4 \qquad [R4]$$

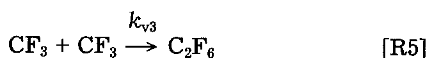

$$CF_3 + CF_3 \xrightarrow{k_{v3}} C_2F_6 \qquad [R5]$$

Ryan and Plumb (14) showed that the above subset yields almost identical results with the more complete set listed in their work. Reactions [R1] and [R2] account for etchant (fluorine atom) production by electron-impact dissociation of the parent gas molecules. The overall production rate is given by $(k_{p1} + 2k_{p2})n_e C_{CF_4}$. Reactions [R3]-[R5] account for volume recombination of the reactive atoms and radicals. The rate constants for these reactions were taken from Ref. (14) and are listed in Table I.

Mass balance equations were written for each of the species F, $CF_i$ ($i$ = 2, 3, 4), neglecting multicomponent diffusion effects and using a pseudobinary diffusion coefficient

$$\frac{\partial C_i}{\partial t} + \mathbf{v} \cdot \nabla C_i = \nabla \cdot (D_{i,CF_4} C \nabla x_i) + G_i \qquad [18]$$

Here $C$ is the total gas concentration, and $C_i$, $D_{i,CF_4}$, and $x_i$ are the concentration, binary diffusivity in $CF_4$, and mole fraction of species i, respectively. The net generation terms $G_i$ are given as follows

$$G_F = (k_{p1}n_e + 2k_{p2}n_e)C_{CF_4} - k_{v1}C_F C_{CF_2} - k_{v2}C_F C_{CF_3} \qquad [19]$$

$$G_{CF_2} = k_{p2}n_e C_{CF_4} - k_{v1}C_F C_{CF_2} \qquad [20]$$

$$G_{CF_3} = k_{p1}n_e C_{CF_4} + k_{v1}C_F C_{CF_2} - k_{v3}C^2_{CF_3} - k_{v2}C_F C_{CF_3} \qquad [21]$$

$$G_{CF_4} = -(k_{p1} + k_{p2})n_e C_{CF_4} + k_{v2}C_F C_{CF_3} \qquad [22]$$

where the rate constants $k_j$ are noted over the corresponding reaction (Eq. [R1]-[R5]). Heterogeneous (surface) reactions enter in the material balance through the boundary conditions. Following Edelson and Flamm (21) and Dalvie *et al.* (4), the heterogeneous reaction set included silicon etching (Eq. [R6]), surface recombination of fluorine atoms [R7], surface recombination of $CF_3$ [R8], and adsorption of $CF_3$ on the silicon surface [R9]

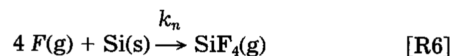

$$4\ F(g) + Si(s) \xrightarrow{k_n} SiF_4(g) \qquad [R6]$$

$$F(g) + CF_3(s) \xrightarrow{k_{s1}} CF_4(g) \qquad [R7]$$

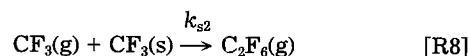

$$CF_3(g) + CF_3(s) \xrightarrow{k_{s2}} C_2F_6(g) \qquad [R8]$$

$$CF_3(g) + Si(s) \xrightarrow{k_{s3}} CF_3(s) \qquad [R9]$$

where the designation (s) implies adsorbed species and (g) implies gaseous-phase species.

Then, the boundary conditions for Eq. [18] are as follows

$$\text{BC1} \begin{cases} \text{Outflow} & -D_{i,CF_4} C \dfrac{\partial x_i}{\partial z} = v_z(C_{if} - C_i) \qquad [23] \\ \text{Inflow} & \dfrac{\partial x_i}{\partial z} = 0 \qquad [24] \end{cases}$$

BC2, 4, 6, 7, 8 $$\frac{\partial x_i}{\partial n} = 0 \qquad [25]$$

BC3

$$-D_{F,CF_4}C\frac{\partial x_F}{\partial z} = k_{s1}\theta C_F + k_n C_F(1-\theta) \quad [26]$$

$$-D_{CF_3,CF_4}C\frac{\partial x_{CF_3}}{\partial z} = k_{s3}(1-\theta)C_{CF_3} + k_{s2}C_{CF_3}\theta \quad [27]$$

$$D_{CF_4,CF_4}C\frac{\partial x_{CF_4}}{\partial z} = k_{s1}\theta C_F \qquad \frac{\partial C_{CF_2}}{\partial z} = 0 \quad [28]$$

BC5

$$\text{Outflow} \qquad \frac{\partial x_i}{\partial z} = 0 \quad [29]$$

$$\text{Inflow} \qquad -D_{i,CF_4}C\frac{\partial x_i}{\partial z} = v_z(C_{if} - C_i) \quad [30]$$

where

$$\theta = \frac{k_{s3}C_{CF_3}}{(k_{s3}+k_{s2})C_{CF_3}+k_{s1}C_F} \quad [31]$$

In the above equations i = F, $CF_2$, $CF_3$, $CF_4$. The etching rate was calculated by

$$r_n = \frac{1}{4}k_n C_F(1-\theta) \quad [32]$$

Here $\theta$ is the fraction of the silicon surface covered by $CF_3$, and $n$ is along the direction normal to the surface. The etching reaction [R6] rate constant as a function of temperature was taken from Flamm *et al.* (15), and is shown in Table I along with the values assumed for the other parameters. BC1 and BC5 are Dankwerts-type (16) boundary conditions at the reactor inlet and exit. BC3 is the reaction boundary condition on the silicon surface, BC2, 4, 6, 7 are the no-reaction boundary conditions on the rest of the reactor walls, and BC8 is a symmetry condition.

In Eq. [19]-[22], the effective dissociation rate constants $k_{p1}n_e$ and $k_{p2}n_e$ are functions of time in a pulsed-plasma mode of operation. In such case, the species concentration distributions are functions of time as well. In the case of continuous-wave reactor operation, the time derivative terms in Eq. [18] were set equal to zero, and the effective dissociation rate constants were taken as time-invariant.

In the case of pulsed-plasma reactor, in order to save computation time, the mass balance equations were averaged over the axial ($z$) direction, resulting in a one-dimensional time-dependent radial dispersion model. In this model, the average gas velocity was used as a function of radius, and the dispersion coefficient was taken equal to the species diffusivity due to the low pressure (17). The surface reaction terms were incorporated into the mass balance by multiplying the surface reaction rate by the surface-to-volume ratio ($1/L$ in this case). The one-dimensional approximation is expected to be good for high aspect ratio reactors (large $R_t/L$) and has been used before (5, 6).

## Method of Solution

The Petrov-Galerkin finite element method was employed to solve the governing equations. Due to the axisymmetric nature of the problem, only half of the reactor domain was considered. The computational domain and the finite element grid used are shown in Fig. 2. The solution procedure was similar to that described before (10). The momentum balance, continuity, and energy balance equations (Eq. [1], [2], and [5], respectively) were solved first. The resulting velocity and temperature distributions were then substituted into the mass balance equation (Eq. [18]) to obtain the species concentration distributions. Etch rate and uniformity were then calculated.

Table II. Reactor dimensions and operating conditions held fixed.

$H$ = 6 cm, $L$ = 4 cm, $W_i$ = 1.75 cm, $W_o$ = 1.5 cm
$R_i$ = 1.25 cm, $R_o$ = 27.5 cm, $R_t$ = 30 cm
$p$ = 0.5 torr, $T_f = T_w$ = 298 K

In the case of pulsed-plasma reactor, the method of lines was used with collocation on finite elements for the spatial discretization. The solution procedure was described elsewhere (11, 22). The periodic steady-state was detected using the same criteria as before (11).

## Results and Discussion

Results are first presented for the cw reactor, operating at steady state, followed by the pulsed-plasma reactor. Table I shows the rate constants and diffusion coefficients used. The rate constants for electron-impact dissociation of the parent molecules (reactions [R1] and [R2]) correspond to a pressure of 0.5 torr. Table II shows the reactor dimensions and operating conditions held fixed. Table III shows the basic value for each of the parameters varied and the range of values examined. The basic parameter values were used unless stated otherwise.

*Continuous-wave (cw) reactor.*—For the cw reactor, full two-dimensional simulations of gas flow velocity, temperature, and species concentration profiles were conducted. The computational domain and the finite element grid used for the simulations are shown in Fig. 2. A finer grid was used near the inlet to the plasma region, since steeper gradients were anticipated in that region. Owing to the axisymmetric nature of the problem, only half of the reactor was considered (BC8 is along the axis of symmetry). The flow streamlines were parallel to the electrode surfaces in the main body of the reactor away from the corner regions. However, recirculating eddies were formed in the corners near the inlet to and exit from the plasma.

Figure 3 shows the fluorine-atom mole fraction distribution in the reactor for the basic parameter values. The plasma was assumed to be confined between the electrodes (*i.e.*, for $z > 0$ in Fig. 3), and the electron density was

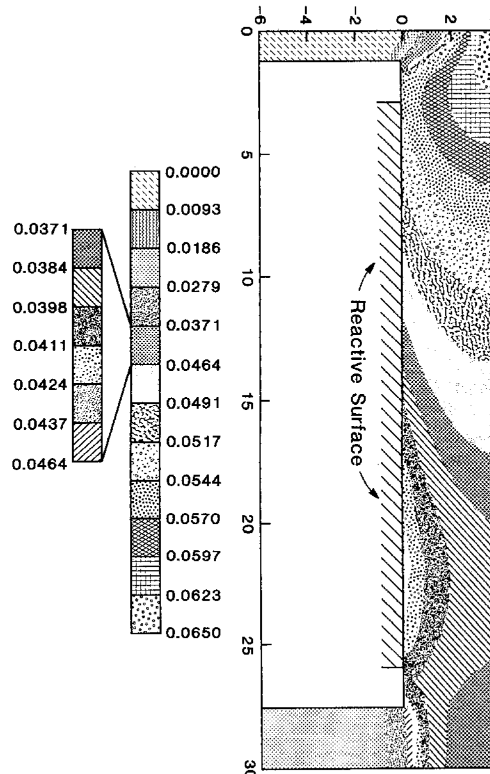


Fig. 3. Fluorine-atom mole fraction distribution in the reactor for the basic parameter values shown in Table III. The expanded scale (mole fractions 0.0371-0.0464) applies to the space given approximately by ($r$ = 15-30 cm, $z > 0$ cm).

assumed to decay rapidly to a zero value outside the plasma. The electron impact dissociation reactions [R1] and [R2] occurred only in the plasma region. Other gas phase reactions occurred in the entire reactor volume.

One observes that the F mole fraction starts out low at the reactor inlet, increases rapidly as the gas enters the plasma region (around $r$ = 0 cm, $z$ = 0 cm), and then decreases as volume recombination (reactions [R3] and [R4]) and etching (reaction [R6]) deplete F. After the gas exits the plasma region, the F mole fraction decreases even further since there is no more source of F. Under the conditions of Fig. 3, the maximum F mole fraction is 6.5%, and this maximum is achieved around the stagnation point ($r$ = 0 cm, $z$ = 4 cm), where the gas is relatively stagnant, resulting in higher degree of dissociation of $CF_4$. The F distribution shown in Fig. 3 would result in an etching rate profile decreasing monotonically along the direction of gas flow, except near the outer edge of the lower electrode, where the F mole fraction shows a slight upward trend. This is a result of local loading, as the bare electrode does not consume fluorine. Hence the excess fluorine diffuses toward the reactive surface serving to enhance the etching rate around the outer periphery of the reactive surface. This phenomenon is entirely similar to the local loading effect observed in single-wafer etchers (18, 10) and in downstream etching reactors (19).

The electron density distribution in plasma reactors is often assumed to correspond to the case of a diffusion-controlled discharge. Then, for a cylindrical container, the following distribution results

$$n_e(r, z) = n_{eo} \sin\left(\frac{\pi z}{L}\right) J_o\left(\frac{2.405r}{R_t}\right) \quad [33]$$

where $J_o$ is the Bessel function of the first kind of order zero. However, in electronegative gases, negative ions partly neutralize the space charge fields, resulting in an increase of the effective electron diffusivity, and a flattening of the electron density profile. In the present work, two electron density distributions were examined: a uniform and a Bessel function distribution. Figure 4a shows the etching rate as a function of radial position, for different gas flow rates, and for a uniform electron density distribution. For low flow rates, the depletion of $CF_4$ is appreciable, resulting in a monotonic decrease of the etching rate along the direction of gas flow. The average etching rate increases and the etching uniformity improves with increasing gas flow rate. The slight increase in the etching rate at the outer periphery of the reactive surface ($r$ = 25 cm) is due to the local loading effect as explained in connection with Fig. 3. The slight local maximum in the etching rate near the inner periphery of the reactive surface, which is observed at high gas flow rates (>500 sccm), is associated with a clockwise eddy driven by the incoming flow. This eddy 'feeds' the region around $r$ = 7.5 cm with gas taken from upstream positions in the plasma which are richer in F. Figure 4b shows the etching rate profile for the case of a Bessel function electron density distribution. The average electron density and other conditions were as in Fig. 4a. One observes much stronger radial etching rate nonuniformities as compared to Fig. 4a. This is a result of higher gas dissociation at the upstream locations because of the higher electron density there. However, the average etching rate is comparable to that of Fig. 4a.

Figure 5a shows the etching rate profile for inward gas flow and for a uniform electron density distribution. Other parameters were at their basic value (Table III). As in the corresponding case of Fig. 4a, gas depletion along the flow direction leads to nonuniform etching. The etching rate decreases along the flow direction, except for a slight upturn near the inner periphery of the reactive surface, which can be attributed to local loading. The case of inward flow with a Bessel electron density profile is illustrated in Fig. 5b. The increasing electron density along the flow direction more than counterbalances the reactant depletion effect, resulting in an inverse etching rate profile when compared to Fig. 5a. The etching rate profile is especially nonuniform at high gas flow rates. The average etching rate was calculated by

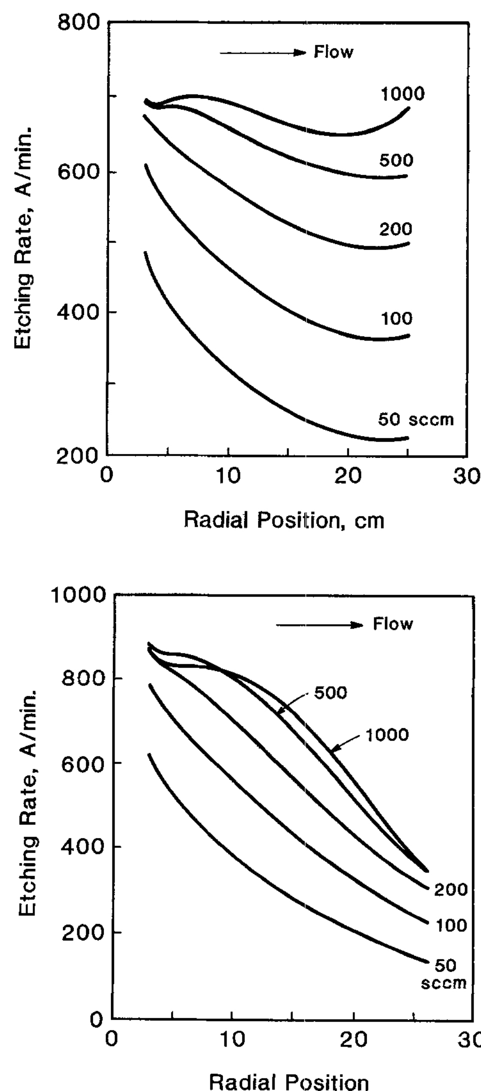


Fig. 4. Etching rate as a function of radial position along the reactive surface, for different gas flow rates, and for outward flow. Electron density distribution was (a) uniform, and (b) Bessel. Other parameters were at their basic value.

$$r_{avg} = \frac{2\int_{R_i+W_i}^{R_o-W_o} r_n r dr}{\{(R_0 - W_0)^2 - (R_i + W_i)^2\}} \quad [34]$$

with $r_n$ given by Eq. [32]. The average etching rate as a function of gas flow rate is shown in Fig. 6 for both outward and inward gas flow, and for uniform electron distribution. The etching rate increases sharply with flow rate at low flow rates and becomes insensitive to flow rate for $Q$ > 600 sccm. At low flow rates, the feed gas is depleted to a high degree, and etching is limited by reactant supply. It is expected that the etching rate would pass through a maximum for high enough values of the flow rate, when convective removal of active species would become the main loss mechanism. Figure 6 suggests that the reactor should be operated at a relatively high flow rate and in the inward flow configuration. However, at high flow rates, a large fraction of the feed gas passes through the reactor unconverted, resulting in poor utilization of the gas and greater expense. For the case of Bessel function electron distribution, the average etching rate as a function of flow rate showed behavior very similar to that of Fig. 6.

Etching uniformity results as a function of flow rate are summarized in Fig. 7. The uniformity index was defined by

$$UI = \frac{r_{max} - r_{min}}{2r_{avg}} \quad [35]$$

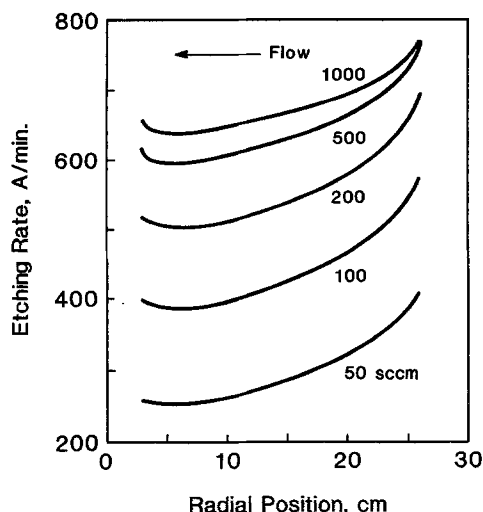


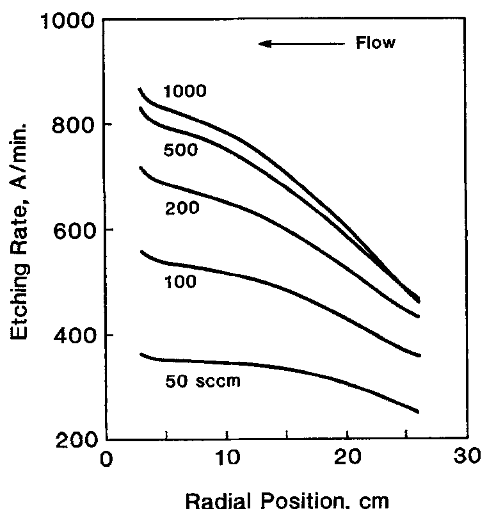


Fig. 5. Etching rate as a function of radial position along the reactive surface, for different gas flow rates, and for inward flow. Electron density distribution was (a) uniform, and (b) Bessel. Other parameters were at their basic value.

A lower $UI$ implies better etching uniformity. Uniformity improves with increasing flow rate except for the case of inward gas flow with a Bessel electron density distribution. For a given flow direction, uniformity becomes generally worse as the electron density distribution turns from uniform to Bessel. If the electron density distribution is a

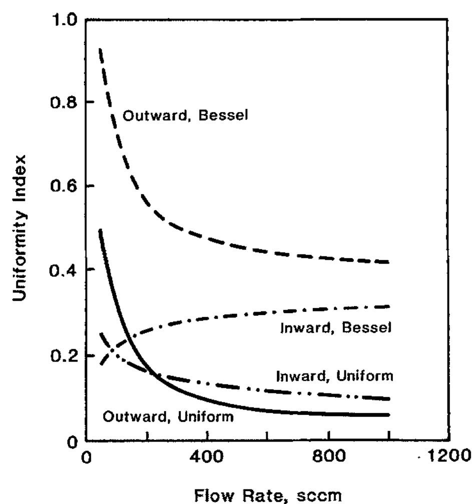


Fig. 7. Uniformity index as a function of flow rate, for different flow directions, and electron density distributions. Other parameters were at their basic value.

Bessel function, inward gas flow is preferable. One observes that, for $Q > 200$ sccm, the case of outward gas flow with uniform electron density yields the best uniformity.

The effective dissociation rate constants $k_{p1}n_e$ and $k_{p2}n_e$ may be varied by varying the power input to the discharge, which, at a constant pressure, mainly affects $n_e$. The effect of power on the etching rate and its profile is shown in Fig. 8, for which parameters were at their basic value. A value of $n_e = 1$ corresponds to an electron density of $10^{10}$ $cm^{-3}$. As power to the discharge ($n_e$) increases, so does the etching rate, albeit the etching rate profile becomes more nonuniform. The $UI$ was found to decrease (improved uniformity) as $n_e$ increased up to a value of 0.25. Further increase of $n_e$ resulted in monotonically increasing $UI$.

Results up to this point were for an isothermal reactor, in which both the reactive surface and the reactor walls were kept at the same temperature (298 K). The effect of the reactive surface temperature is shown in Fig. 9 for outward (Fig. 9a) and inward (Fig. 9b) flow, respectively. As expected, the etching rate increases with temperature. However, as temperature increases, the etching nonuniformity becomes severe because of substantial etchant depletion along the flow direction. In addition, the local loading effect at the downstream edge of the etching surface becomes increasingly important with increasing temperature. This is because of the greater disparity in reactivity between the etching surface and the surrounding electrode (18). The uniformity index as a function of temperature is shown in Fig. 10. The uniformity becomes worse as

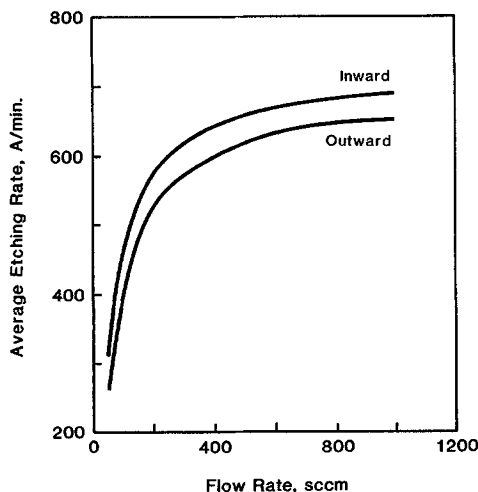


Fig. 6. Average etching rate as a function of flow rate for inward and outward flow. Other parameters were at their basic value.

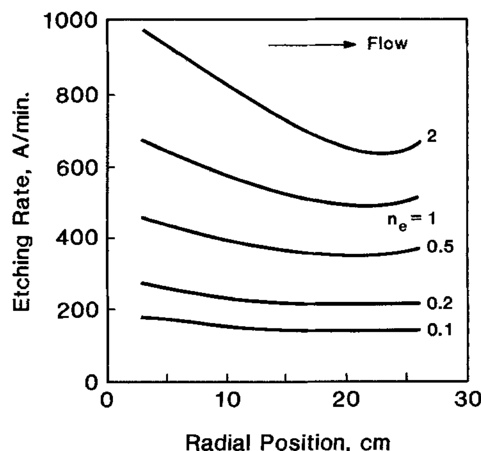


Fig. 8. Etching rate as a function of radial position along the reactive surface for different values of the effective dissociation rate constant (power). Other parameters were at their basic value.

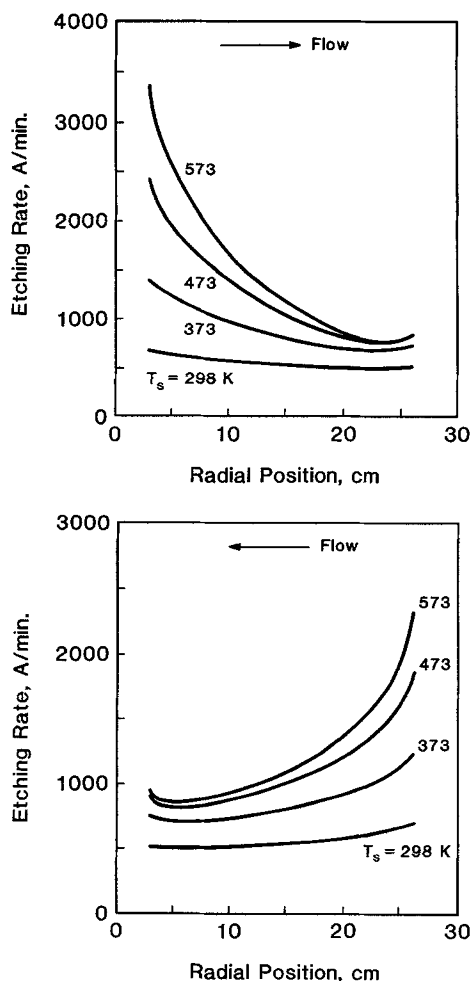


Fig. 9. Etching rate as a function of radial position along the reactive surface for different values of the silicon surface temperature, and for (a) outward flow, and (b) inward flow. Other parameters were at their basic value.

temperature increases, and the outward flow configuration results in better uniformity as compared to inward flow. As was seen in Fig. 6, at low substrate temperature (298 K), inward flow results in slightly higher average etching rate as compared to outward flow. However, for higher temperature the outward flow gives better etching rate (compare Fig. 9a and b). Combining the results of Fig. 7, 9, and 10, one concludes that, for relatively high substrate temperature and gas flow rate, the outward flow configuration yields the best etching rate and uniformity results, under the conditions examined.

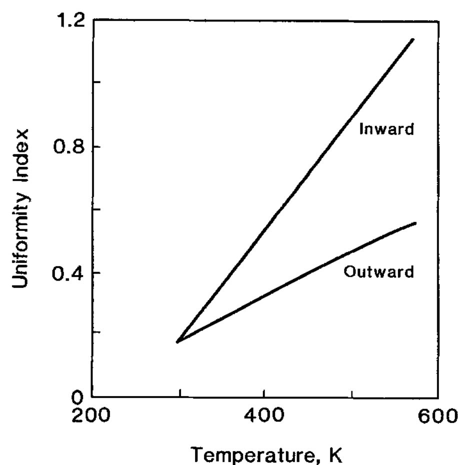


Fig. 10. Uniformity index as a function of the silicon surface temperature. Conditions were as in Fig. 9.

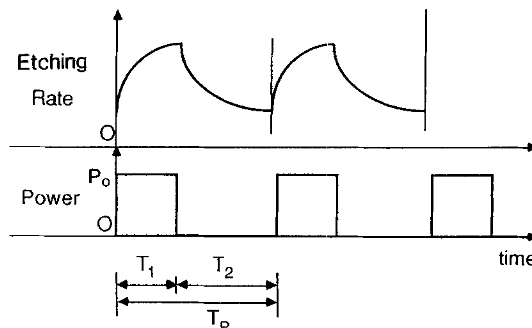


Fig. 11. Square-wave modulation of the power input to the plasma, and schematic of time response of the average etching rate.

*Pulsed-plasma reactor*.—In the pulsed-plasma reactor, power to the plasma is modulated at a frequency much lower than the common radio frequencies used to excite the discharge. A schematic of the power modulation and the resulting etching rate are shown in Fig. 11. The pulse period is $T_p$ and power is applied only for time $T_1$ during a period. During the plasma-on fraction of the cycle, the common frequency of 13.56 MHz may be used to affect efficient gas dissociation and to avoid intense ion bombardment or charging of dielectric surfaces. The duty cycle is defined as $f_d\% = 100\ T_1/T_p$. After a sufficient number of cycles, a periodic steady state will be reached for which the values of the dependent variables (*e.g.*, etching rate) will be the same at time $t$ and time $(t + nT_p)$ where $n$ is a positive integer. It is this periodic steady state which is of interest in the present work. In the pulsed-plasma reactor, and for the pulsing frequencies of interest, the rate coefficients for electron-neutral reactions can no longer be taken as time-independent. In the present work, it was assumed that the effective dissociation rate constant is completely modulated according to the applied power waveform. This appears to be a good assumption for the $CF_4$ plasma (20). The modulation of the etchant production rate constant introduces a temporal variation in the species concentrations, and in turn in the etching rate. However, neglecting volume expansion due to reaction and gas heating, the fluid velocity and temperature distributions may be assumed to be time-independent. The problem is then to first solve for the time-independent fluid velocity and temperature distributions, and then substitute into the time-dependent mass balance equations to solve for the concentration and etching rate distributions. This approach was followed in analyzing a two-dimensional pulsed-plasma single-wafer etcher (10).

In order to save computation time, an approximation was used in the present case. This approximation is based on the fact that for relatively high aspect ratio ($R_t/L$) reactors, a one-dimensional radial dispersion model may be a good representation of the real two-dimensional reactor. The surface reaction terms were accommodated in the one-dimensional model by multiplying by the surface-to-volume ratio. Dankwerts-type boundary conditions were applied in the radial direction. A one-dimensional axial dispersion model was used to describe a pulsed-plasma CVD reactor with recycle (11). A one-dimensional dispersion model of a radial flow reactor of the type examined in the present work has also been reported (5, 6). A comparison of the predictions of the full two-dimensional model with the one-dimensional radial dispersion approximation is shown in Fig. 12. Parameters were at their basic value. One observes generally good agreement except for edge effects. The disagreement around the edges of the reactive surface is understood, because the Dankwerts boundary conditions used for the one-dimensional model are not as good of an approximation when applied at the plasma edge.

The spatial and temporal variation of the etching rate is shown in the three-dimensional plot of Fig. 13. Parameters were at their basic value. The pulse period was 0.01 s, and the duty cycle was 50%. The two graphs correspond to the same 3-D plot viewed from two different angles. The plot

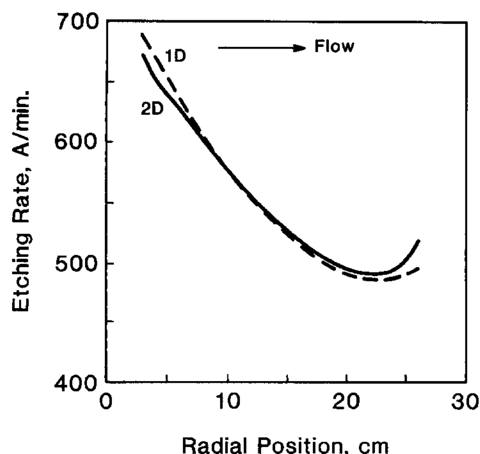


Fig. 12. Comparison of the etching rate radial profile obtained by the two-dimensional model and the one-dimensional radial dispersion approximation. Parameters were at their basic value.

pictures the periodic steady state achieved after a number of cycles. As expected, the etching rate increases during the power-on fraction of the cycle, attains a maximum, and starts decreasing as soon as the power is turned off. One observes that etching continues even after extinction of the plasma. This is expected for values of the pulse period which are not much longer than the fluorine atom lifetime. The latter depends on the rate constants of the F loss reactions and on the gas flow rate. Under the present conditions, the volume recombination reactions [R3] and [R4] are the most significant loss mechanism for F. The time- and space-averaged etching rate under the conditions of Fig. 13 is 385 Å/min. When prorated by the duty cycle, the average etching rate becomes 385/0.5 = 770 Å/min. The average etching rate of the cw reactor under otherwise the same conditions is 525 Å/min. One observes that the etching rate achieved with the pulsed-plasma reactor, when prorated by the duty cycle, is higher than the corresponding rate of the cw reactor. The pulsed-plasma reactor can also yield better uniformity as discussed below.

In order to better understand the origin of the uniformity improvement in the pulsed-plasma reactor, it is instructive to examine the parent gas ($CF_4$) concentration profiles

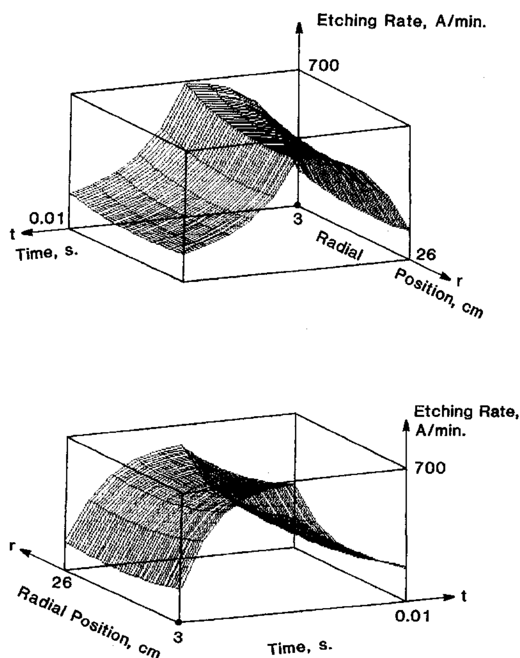


Fig. 13. Spatial and temporal variation of the etching rate in a pulsed-plasma reactor. Pulse period was 0.01 s and duty cycle was 50%. Other parameters were at their basic value.

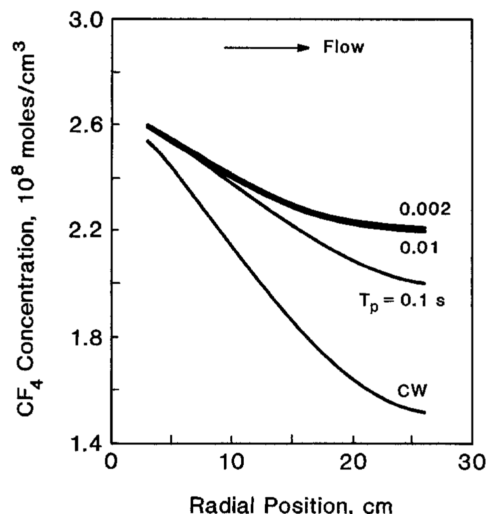


Fig. 14. Radial concentration profiles of $CF_4$ in a pulsed-plasma reactor for a duty cycle of 50%. The cw reactor profile (at $z = 0$) is also shown. Other parameters were at their basic value.

along the reactor radius, shown in Fig. 14. Other conditions were at their basic value, and the duty cycle was 50%. One observes that the depletion of the parent gas is substantially reduced by pulsing the plasma. During the plasma-off fraction of the cycle, $CF_4$ is replenished by fresh feed and especially by the volume recombination reactions [R3] and [R4] which regenerate $CF_4$. The concentration profile becomes smoother as the pulse period decreases. Minimizing the depletion of the parent gas results in better etching uniformity. Another method to minimize the gas depletion is to increase the flow rate. However, this approach also results in poor gas utilization, since large quantities of the gas pass through the reactor unconverted. Figure 15 shows the time-averaged etching rate distribution along the reactor radius. The cw profile is also shown. Conditions were as in Fig. 14. The etching rate profile becomes much smoother in the pulsed-plasma reactor, in accordance with the discussion of Fig. 14. The etching rate increases with decreasing pulse period. This is because, with short pulse periods, the fluorine atom concentration will have less chance to decay during the plasma-off fraction of the cycle. The etching rate appears to saturate for very short pulse periods. The saturation value depends on the duty cycle.

For a given pulse period, the time- and space-averaged etching rate was found to increase with duty cycle, since etchant production occurs for a larger fraction of time as

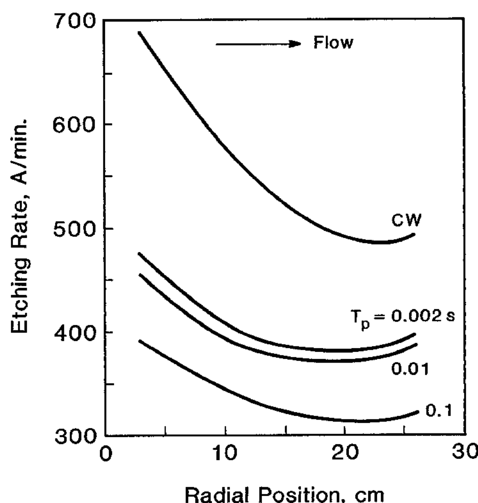


Fig. 15. Time-averaged etching rate radial profiles in a pulsed-plasma reactor, for a duty cycle of 50%. The cw reactor profile is also shown. Other parameters were at their basic value.

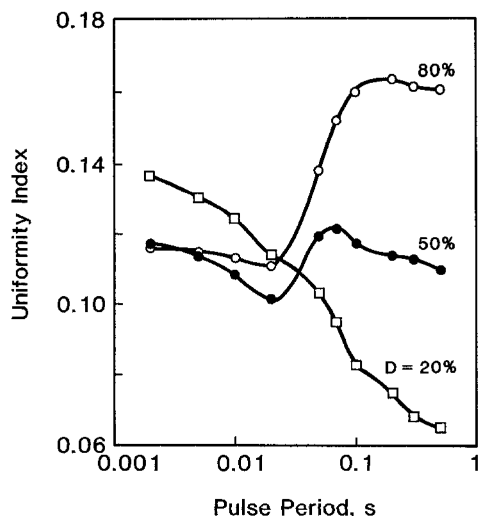


**Fig. 16. Uniformity index as a function of the pulse period for different duty cycles. Other parameters were at their basic value.**

the duty cycle increases. Further, for a given duty cycle, the etching rate attained limiting values for very long and very short values of the pulse period. Similar behavior was observed in the analysis of a pulsed-plasma CVD reactor (11). The uniformity index (*UI*) as a function of pulse period for different values of the duty cycle is shown in Fig. 16. The points are calculated *UI* values and the solid lines are drawn to guide the eye. The etching uniformity appears to improve (lower *UI*) with increasing pulse period for low duty cycles (20%). However, the opposite is true for high duty cycles (80%) and long periods. From the etching rate point of view, a high duty cycle and a short pulse period are desirable. These happen to be the conditions which also result in improved etching uniformity.

The uniformity index as a function of flow rate is shown in Fig. 17. One observes that pulsing of the plasma is most beneficial at low flow rates, which also correspond to high depletion of the precursor gas. For otherwise basic parameter values, it was found that for flow rates less than 100 sccm, the pulsed-plasma reactor etching rate was nearly the same as the cw reactor etching rate (without prorating by the duty cycle). In addition, at these low flow rates, the pulsed-plasma reactor offers an improvement in uniformity of over 50%, as seen in Fig. 17. It appears that, at high flow rates, the pulsed-plasma reactor offers no advantage from the etching rate and uniformity point of view. However, high flow rates result in low utilization of the parent gas.

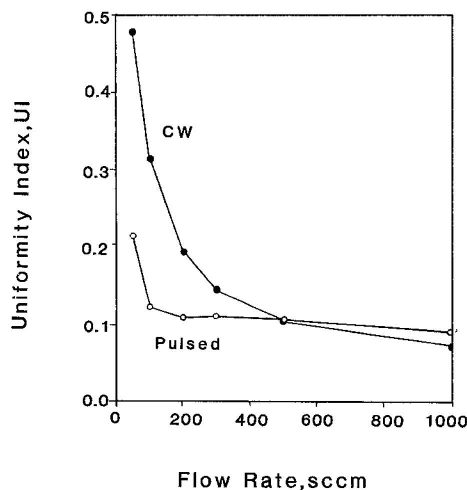


**Fig. 17. Uniformity index as a function of the flow rate in a cw reactor and a pulsed-plasma reactor. Other parameters were at their basic value.**

**Table III. Operating conditions varied.**

| Quantity | Basic value | Range examined |
|---|---|---|
| Flow rate, $Q_o$ | 200 sccm | 50-1000 sccm |
| Si temperature, $T_s$ | 298 K | 298-573 K |
| Flow direction | Outward | Inward |
| Electron distribution | Uniform | Bessel |
| Electron density | $10^{10}$ cm$^{-3}$ | $10^9$-2 $10^{10}$ cm$^{-3}$ |
| Pulse period | 0.01 s | 0.002-0.1 s |
| Duty cycle | 50% | 20-80% |

## Summary and Conclusions

A numerical simulation of silicon etching using tetrafluoromethane in a radial flow reactor was conducted. Finite element methods were employed to solve for the two-dimensional fluid velocity, temperature, and species concentration distributions in a continuous-wave (cw) reactor. The effect of gas flow rate, flow direction, electron density and its distribution, and temperature, on the etching rate and uniformity was examined. The range of parameter values studied is shown in Table III. In the range of flow rates examined (50-1000 sccm), the etching rate increased monotonically with flow rate. The etching uniformity improved with increasing flow rate except for inward flow with a Bessel electron density distribution. The etching rate increased by increasing the effective etchant production rate constant (power to the plasma). The uniformity index passed through a minimum (optimum uniformity) as power to the plasma varied. The etching rate increased, but the uniformity degraded by increasing the silicon surface temperature. At low substrate temperature (298 K), inward flow resulted in higher average etching rate when compared to outward flow. However, the trend reversed for higher substrate temperature. For flow rate higher than 200 sccm, outward flow with a uniform electron density gave the best uniformity.

A one-dimensional time-dependent radial dispersion model was also formulated and was used to study a pulsed-plasma reactor. The one-dimensional model was found to yield etching rate results in reasonable agreement with the results of the full two-dimensional model. The effect of pulse period and duty cycle on etching rate and uniformity was studied. The etching rate of the pulsed-plasma reactor, when prorated by the duty cycle, was higher than that of the cw reactor. The etching rate increased with decreasing pulse period and with increasing duty cycle. The etching rate saturated for very short and very long pulse periods. It was further found that, at high duty cycles, the etching uniformity improved by decreasing the pulse period. Under conditions which would result in high depletion of the precursor gas in a continuous-wave reactor (*i.e.*, for low flow rates), the pulsed-plasma reactor can offer substantial improvement in uniformity without sacrificing the etching rate.

The present model is only an approximation of a real radial flow reactor. For example, the lower electrode was assumed to be completely covered with silicon (except for the area around the edges). In practice, only discrete areas of the lower electrode are covered by wafers. Hence, the present model yields information on the wafer-to-wafer uniformity, but no information on the intrawafer uniformity. The latter was examined in Ref. (7). In addition, the gas-phase and especially the surface reaction kinetics is based on inexact knowledge. For example, the adsorption-reaction-desorption of $CF_x$ on the silicon surface is poorly understood. Nevertheless, the present model may be used to draw at least qualitative information on the response of a radial flow reactor to variations in the operating conditions. Furthermore, the pulsed-plasma reactor concept may be beneficial for radial flow reactors used for either etching or deposition. Clearly, the model coupled with experimental observations can be a more useful tool for analyzing plasma reactors.

## Acknowledgments

We are grateful to the National Science Foundation (CBT-8708908) for financial support, and to the Houston

Advanced Research Center (HARC) for an NEC SX-2 supercomputer-time grant. S.-K. Park was partially supported by a scholarship from the Ministry of Education, Republic of Korea.

Manuscript submitted July 30, 1990; revised manuscript received Dec. 6, 1990.

*University of Houston assisted in meeting the publication costs of this article.*

LIST OF SYMBOLS

| | |
|---|---|
| $C$ | total gas concentration, mol/cm$^3$ |
| $C_i$ | concentration of species i, mol/cm$^3$ |
| $C_{if}$ | feed concentration of species i, mol/cm$^3$ |
| $c_p$ | heat capacity at constant pressure, cal/(g-K) |
| $D_{i,CF_4}$ | diffusivity of species i in $CF_4$, cm$^2$/s |
| $f_d$ | duty cycle, % |
| $G_i$ | net generation rate of species i, mol/(s-cm$^3$) |
| $G_h$ | generation rate of heat, cal/(s-cm$^3$) |
| $g$ | gravitational acceleration, cm/s$^2$ |
| $H$ | length of central port (see Fig. 1), cm |
| $k_n$ | etching rate constant (reaction R6), cm/s |
| $k_{p1}$, $k_{p2}$ | etchant production rate constants (reactions R1 and R2), cm$^3$/s |
| $k_{v1}$, $k_{v2}$, $k_{v3}$ | volume recombination rate constants (reactions R3-R5), cm$^3$/(mol-s) |
| $k_{s1}$, $k_{s2}$, $k_{s3}$ | surface recombination rate constants (reactions R7-R9), cm/s |
| $L$ | interelectrode spacing, cm |
| $n_e$ | electron density, cm$^{-3}$ |
| $p$ | pressure, dynes/cm$^2$, torr |
| $Q$ | gas flow rate at reactor conditions, cm$^3$/s |
| $Q_o$ | feed gas flow rate, sccm |
| $R_i$ | radius of central port (see Fig. 1), cm |
| $R_o$ | radius of lower electrode (see Fig. 1), cm |
| $R_t$ | radius of upper electrode (see Fig. 1), cm |
| $r$ | radial coordinate, cm |
| $r_n$ | etching rate, Å/min |
| $r_{avg}$ | average etching rate, Å/min |
| $T$ | gas temperature, K |
| $T_s$ | silicon surface temperature, K |
| $T_o$ | reference temperature, 298 K |
| $T_f$ | feed gas temperature, K |
| $T_p$ | pulse period, s |
| $UI$ | uniformity index (Eq. [35]) |
| $\mathbf{v}$ | fluid velocity vector, cm/s |
| $v_z$ | axial velocity component, cm/s |
| $v_r$ | radial velocity component, cm/s |
| $v_{avg}$ | average gas velocity in central port, cm/s |
| $v^*_{avg}$ | average gas velocity in outer port, cm/s |
| $W_i$ | width of inner ring of lower electrode not covered by silicon (see Fig. 1), cm |
| $W_o$ | width of outer ring of lower electrode not covered by silicon (see Fig. 1), cm |
| $x_i$ | mole fraction of species i |
| $z$ | axial coordinate, cm |

Greek

| | |
|---|---|
| $\theta$ | surface coverage by $CF_3$ |
| $\kappa$ | gas thermal conductivity, cal/(cm-s-K) |
| $\mu$ | gas viscosity, g/(cm-s) |
| $\rho$ | gas density, g/cm$^3$ |
| $\tau$ | stress tensor (Eq. [3]) |

REFERENCES

1. "Plasma Etching: An Introduction," D. M. Manos and D. L. Flamm, Editors, Academic Press, San Diego, CA (1989).
2. "Plasmas Processing for VLSI," Vol. 8, N. G. Einspruch and D. M. Brown, Editors, Academic Press, New York (1984).
3. A. R. Reinberg, *J. Electron. Mater.*, **8**, 345 (1979).
4. M. Dalvie, K. F. Jensen, and D. B. Graves, *Chem. Eng. Sci.*, **41**, 653 (1986).
5. S. P. Venkatesan, I. Trachtenberg, and T. F. Edgar, *This Journal*, **134**, 3194 (1987).
6. S. P. Venkatesan, T. F. Edgar, and I. Trachtenberg, *ibid.*, **136**, 2532 (1989).
7. H. G. Stenger, Jr., H. S. Caram, C. F. Sullivan, and W. M. Russo, *AIChE J.*, **33**, 1187 (1987).
8. H. G. Stenger, Jr. and G. S. Akiki, *Mat. Res. Symp. Proc.*, **68**, 267 (1986).
9. C.-S. Yoo and A. G. Dixon, *AIChE J.*, **35**, 995 (1989).
10. S.-K. Park and D. J. Economou, *This Journal*, **137**, 2624 (1990).
11. S.-K. Park and D. J. Economou, *ibid.*, **137**, 2103 (1990).
12. R. C. Weast and M. J. Astle, Editors, "CRC Handbook of Chemistry and Physics," 62nd edition, CRC Press, Boca Raton, FL (1981).
13. I. C. Plumb and K. R. Ryan, *Plasma Chem. Plasma Proc.*, **6**, 205 (1986).
14. K. R. Ryan and I. C. Plumb, *ibid.*, **6**, 231 (1986).
15. D. L. Flamm, V. M. Donnelly, and J. A. Mucha, *J. Appl. Phys.*, **52**, 3633 (1981).
16. P. V. Dankwerts, *Chem. Eng. Sci.*, **2**, 1 (1953).
17. G. I. Taylor, *Proc. R. Soc. London, Ser. A*, **219**, 186 (1953).
18. D. J. Economou, S.-K. Park, and G. D. Williams, *This Journal*, **136**, 188 (1989).
19. S.-K. Park and D. J. Economou, *J. Appl. Phys.*, **66**, 3256 (1989).
20. S. G. Hansen, G. Luckman, and S. D. Colson, *Appl. Phys. Lett.*, **53**, 1588 (1988).
21. D. Edelson and D. L. Flamm, *J. Appl. Phys.*, **56**, 1522 (1984).
22. S.-K. Park, "Analysis of Glow Discharge and Transport Phenomena in Plasma Reactors," Ph.D. Thesis, University of Houston, Houston, TX (1990).